PHYSICAL REVIEW E **80**, 015301(R) (2009)

Flow-field dynamics during droplet formation by dripping in hydrodynamic-focusing microfluidics

D. Funfschilling,[1,*] H. Debas,[1] H.-Z. Li,[1] and T. G. Mason[2]
[1]*LSGC, Nancy-Université, CNRS, 1 rue Grandville, BP20451, F-54001 Nancy, France*
[2]*Department of Physics and Astronomy, UCLA, Los Angeles, California 90095, USA*
(Received 6 May 2008; revised manuscript received 30 March 2009; published 6 July 2009)

Using microscopic particle image velocimetry, we examine the flow field around an oil droplet as it is formed by hydrodynamic focusing in an aqueous solution using a pressure-driven cross-channel microfluidic device. By detecting the temporal dependence of the instantaneous flow fields of the continuous phase in the dripping regime, we show that shear is not the primary mechanism that initiates droplet formation in our low flow rate and moderate capillary number experimental conditions. Instead, the advancing finger of oil partially and temporarily plugs the outlet channel, creating a pressure difference that builds up and is released when water from the side channels pushes the tip of the finger into the outlet channel, thereby facilitating the birth of the droplet by interfacial pinch-off that is primarily initiated by an extensional flow.

DOI: 10.1103/PhysRevE.80.015301 PACS number(s): 47.61.Jd, 47.80.Cb, 47.57.jb

Many industrial methods of producing emulsions and foams are bulk processes based on the application of significant viscous stresses through shear and extensional flows. Primarily due to inhomogeneities of the flows and lack of control over the emulsification process, the resulting droplet size distribution can often be polydisperse. Although polydispersity can sometimes be desirable in industrial applications, controlling the droplet size distribution is generally advantageous.

Droplets created using controlled flows can be highly uniform, as demonstrated using a microfluidic flow-through Couette emulsification apparatus that creates a uniform shear flow [1]. Following the work of Ganan-Calvo [2], the production of uniform droplets and bubbles has been examined in *T* [3] and hydrodynamic-focusing [2,4–8] geometries. This geometry provides a convenient means of creating droplets that have extremely low size polydispersity [2,7] over a large range of droplet sizes by varying the flow rates of the continuous and dispersed phases using syringe pumps or pressure drive [9]. Massive parallelization of a flow-focusing geometry is also very promising for industrial applications [10]. Given this context, it is important to understand the local flow fields around droplets formed in the various stages of rupturing in a simple hydrodynamic focusing geometry in the dripping regime.

In order to directly measure the dynamics of the flow during rupturing, we map the two-dimensional flow field of the liquid aqueous phase around a droplet as it separates from an extending finger using microscopic particle image velocimetry (μPIV) in the midplane. μPIV is a relatively new technique for measuring the instantaneous flow-field in a complete plane [11], providing key details about the hydrodynamics taking place. The microfluidics device consists of a double-polished silicon wafer having thickness $h=250$ μm that has been patterned and etched by deep reactive ion etching (DRIE) sandwiched between two glass plates and permanently fused together by anodic bonding [6]. Two side channels intersect the central straight entrance channel, forming a hydrodynamic focusing geometry. The dispersed phase (oil) is injected into the central channel, and the continuous phase (an aqueous surfactant solution) is injected into the two side channels. The two liquids are driven by constant pressure gravity feed [9]. Both central and side channels are $l=270$ μm wide, so they all have nearly a square cross section. A top view of the intersection of main and side channels of the device, while dripping oil droplets is shown in Fig. 1.

As inputs into this device, we select two immiscible liquids that have low mutual solubility. The dispersed phase is polydimethylsiloxane (PDMS) silicone oil (Dow Corning 200R). Its viscosity is $\mu=6.0$ mPa s, and its density is $\rho=0.913$ g/cm^3 at 20 °C. The continuous phase is a 2 wt % aqueous surfactant solution of sodium dodecyl sulfate (SDS) (Amersco) in distilled water. The reported critical micelle concentration (CMC) of SDS is about 7 mM at 20 °C [12]. Hence, the concentration of SDS we use is about ten times the CMC so there is ample surfactant that will rapidly adsorb on any newly created oil-water interfaces. The fluids flow from liquid reservoirs that have heights above the microfluidic device of 7.0 and 8.0 cm for the dispersed and continuous phases, respectively, corresponding to driving pressures of 690 and 720 Pa. The interfacial tension between silicone

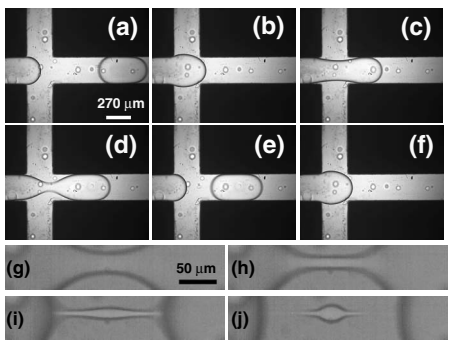

FIG. 1. High-speed optical microscopy image sequence of droplet formation by dripping in a microfluidic hydrodynamic focusing device: (a) $t_1=0$, (b) $t_2=98$, (c) $t_3=114$, (d) $t_4=120$, (e) $t_1'=122$, and (f) $t_2'=216$ (in ms). The channel width is 270 μm. Details of the neck rupturing and the formation of a satellite droplet: panels (g)–(j) (0.1 ms apart).

*denis.funfschilling@ensic.inpl-nancy.fr

oil and the aqueous SDS solution is $\lambda = 15.8$ mN/m measured using a pendant drop technique on a Tracker apparatus (I. T. Concept). In competitive wetting experiments, we find that the aqueous surfactant solution strongly wets the glass surfaces and tends to displace the silicone oil. Although the definition of a contact angle is dubious when competitive wetting occurs, if one were to measure a contact angle of an oil droplet in the presence of water wetting the silicon, this angle would be in excess of 130°.

The velocity flow fields of the continuous phase are measured using a μPIV system (Dantec Dynamics). Calibrated latex microspheres of 0.88 μm diameter (Estapor) are dispersed as seed particles in the continuous phase at a volume fraction of $\phi = 10^{-4}$. The time interval between images in a pair is typically $\Delta t = 100$ μs, the stroboscopic illumination time is 50 μs, and pairs of images are taken at 7 Hz at 2048×2048 pixels^2 resolution (1.5×1.5 mm^2). From each image pair, 63×63 velocity vectors are calculated, with a spacing between vectors of 23.7 μm. By controlling the focus of the camera, the flow field is measured at the midheight of the channel. High-speed movies of dripping are also obtained (CamRecord, Optronix); image analysis using MATLAB (MathWorks) provides droplet volumes and shapes. Because the steady-state dripping is highly reproducible and periodic, we can match the flow fields obtained using μPIV at different stages during rupturing to the images of the droplet interfaces determined using the fast camera.

For a single set of conditions that exemplify the dripping regime [13], we study the flow fields before, during, and after droplet pinch-off. The time-averaged flow rates of the continuous phase and oil are 1.39 and 0.185 μL/s, respectively. Droplets of 2.54×10^{-11} m^3 are created at a rate of 7.3 Hz. The mean radius is $\bar{r} = 182$ μm with a narrow standard deviation of $\delta r = 1.6$ μm. Each time a primary droplet detaches, one smaller satellite droplet of ≈ 30 μm diameter is formed where the neck ruptures. The Reynolds number is $\mathrm{Re} = \frac{\rho U h}{\mu} \approx 5$, where U is the mean velocity of the detached primary droplet.

High-speed imaging of droplets formed by controlled dripping provides a sequence of important morphological events (Fig. 1). A finger of oil with a tip that roughly resembles the shape of a half dome (time t_1) extends from the main inlet channel (left) into the intersecting region with the two side channels (top and bottom) until it reaches the edges of the exit channel (right) (time t_2). Thereafter, the tip of the finger partially plugs the exit channel [Figs. 1(c) and 1(d)]. A "plug" is a finger that almost contacts all four walls but does not wet the walls because of the presence of a thin film of continuous phase between the finger and the wall [14]. Subsequently, a neck begins to form at time t_3. It thins until it ruptures through a capillary instability at time t_4. As the primary droplet detaches, the neck ruptures in a manner that leads to the formation of a single satellite droplet [Figs. 1(g)–1(j)]. Neck rupturing typically occurs in less than 100 μs. A typical capillary number $\mathrm{Ca} = \frac{\mu U}{\gamma}$, which provides a dimensionless measure of the ratio between bulk viscous and interfacial stresses, is in the range $0.0011 < \mathrm{Ca} < 0.0155$. Obviously, during the last stage of interfacial pinch-off when the droplet is formed, a local capillary number of the extended neck must become comparable to unity in order for the pinch-off to occur.

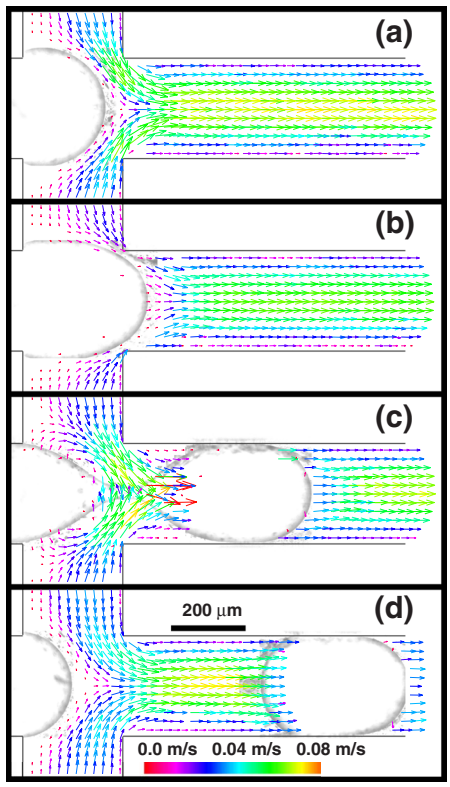

FIG. 2. (Color online) μPIV measurements reveal the velocity flow fields (color-coded arrows) in the center plane of the channels and around the oil-water interfaces as a droplet is formed. (a) Time $t = 50$ ms, Ca=0.0011, (b) $t_2 = 98$ ms, Ca=0.092, (c) $t_4 = 120$ ms, Ca=0.0155, and (d) $t_1' = 122$ ms, Ca=0.0011. For clarity, the channel walls and outline of the interface of the droplets have been superimposed.

The μPIV velocity fields are associated with the liquid interfaces at the appropriate phase in the cycle of dripping and shown in Fig. 2 for an entire cycle. The instantaneous flow rate calculated from the flow field reaches a minimum around t_2 and then increases again as the neck forms until rupturing occurs. Thus, the flow is restricted as the droplet is being formed; a difference in pressure builds up when the finger mostly plugs the exit channel. During the formation of each bubble, it has been hypothesized that gas entering the outlet channel constricts the flow, leading to higher pressure in the entrance channel [4]. This increase in pressure has been confirmed by simulations using the volume of fluid method [15]. The μPIV measurements of the continuous phase flow fields in Fig. 2 are consistent with this overall picture.

In addition, μPIV also reveals how the interfacial tension after the rupturing event alters the local flow fields in the intersecting cross-channel region. Immediately after pinch-off, one interface moves toward the entrance channel and the other interface moves toward the center of mass of the newly formed droplet (i.e., the exit channel). The simultaneous retraction of interfaces in opposite directions temporarily creates a stagnation point between the retracting finger and the free-flowing droplet. This stagnation point driven by interfacial tension is directly revealed by μPIV measurements.

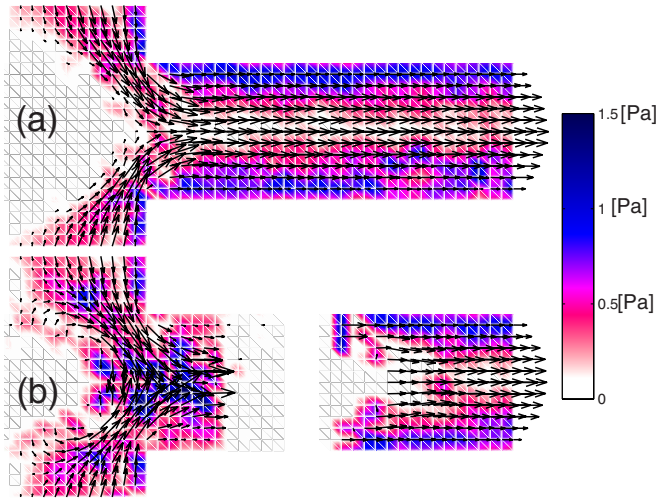

FIG. 3. (Color online) Magnitude of the stress field superimposed with the velocity (a) $t=50$ ms, as Figs. 2(a) and 2(b) $t_4=120$ ms, as Fig. 2(c).

After the primary droplet detaches and the much smaller satellite droplet is formed through a capillary instability, this satellite droplet accelerates away from the stagnation point downstream. Thus, the satellite droplet rapidly catches up with the trailing edge of the primary droplet and thereafter remains closely behind it. This behavior of the satellite droplet directly corresponds to the time-resolved flow maps of the continuous phase.

Before rupturing occurs, the velocity vectors around the neck are essentially perpendicular to the oil/water interface, and there is no noticeable velocity gradient parallel to the interface. This indicates that the shear components in the stress tensor are quite small initially and the droplet is pushed into the exit channel, creating a dominantly extensional flow in the vicinity of the neck. In Fig. 2(c), the oil finger begins to reorganize its shape to become a spherical cap even before the rupture of the neck due to the local flows caused by surface tension.

Moreover, there is essentially no slip at the interface, since the velocities near the surfactant-covered oil-water interfaces become greatly reduced (Fig. 2). At such high concentrations of SDS above the CMC, the interfacial elasticity of the adsorbed surfactant is sufficient to resist the viscous stresses created by flow near the interfaces. The velocity gradient given by the average strain rate extracted from the flow field measured by μPIV is around 400 s^{-1} for Fig. 2(a). This corresponds to shear stresses on the interface of around 0.4 Pa [Fig. 3(a)]. Before reaching the edges of the exit channel, the shear stresses increase up to around 2 Pa. Assuming that the droplet is a half dome, the estimated pressure difference based on Laplace's law is $\Delta P=2\gamma/r=140$ Pa, about 2 orders of magnitude larger than the shear stress on the interface. Thus, the droplet is not significantly deformed due to shear stresses. We estimate the static pressure at the tip of the finger [Fig. 2(a)] to be 3.2 Pa using Bernoulli's relation. The stresses are therefore separated successively by roughly an order of magnitude: surface tension-driven stress > static pressure > shear stress. As the advancing finger enters the outlet channel, water flow around it occurs primarily near the corners of the square channel, not at the midplane where our μPIV measurements are made.

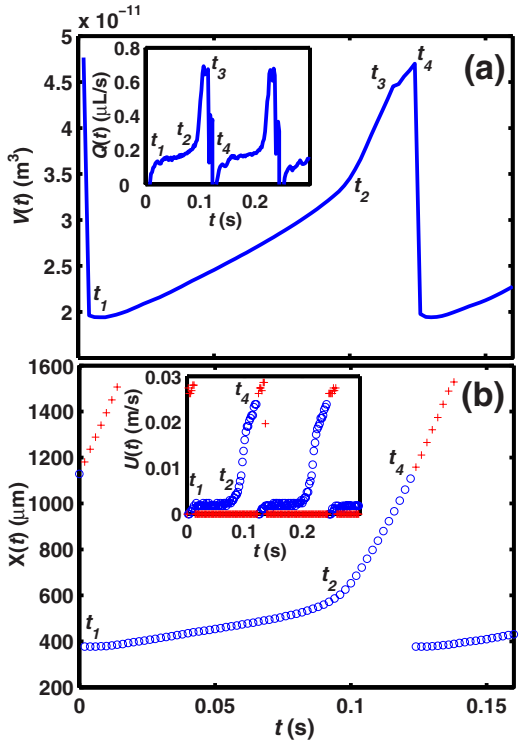

FIG. 4. (Color online) Periodic variation in flow parameters during dripping: (a) $V(t)$ volume of the oil finger versus time (measured relative to the end of the entrance channel). Inset: $Q(t)$ volume flow rate of the oil phase. (b) Temporal dependence of the position $X(t)$ of the tip of the oil finger or droplet (measured relative to the end of the entrance channel). Inset: velocity $U(t)$ of the leading tip of the finger or droplet during a cycle: finger (blue circles: ○) and droplet (red plus: +)

Due to the constant-pressure drive, the flow rates of the aqueous solution and the oil vary during the formation of a droplet, leading to substantial changes in the velocity flow fields during one dripping cycle. The growth velocity of the finger is directly linked to the periodic volume flow rate $\dot{Q}$ of the oil [Fig. 4(a) inset]. The growth of the finger consists of three steps: (1) a slow step from t_1 to t_2 where the finger reaches the edges of the exit channel; (2) a rapid increase from t_2 to t_3 where the neck begins to form; and (3) a slower growth from t_3 until rupturing occurs at t_4. The minimum oil flow rate corresponds to the maximum aqueous solution flow rate at time t_1. The minimum aqueous solution flow rate occurs at time t_2, whereas the oil maximum occurs at time t_3.

These μPIV measurements show that, during the formation of the finger and plugging of the exit channel, the pressure-driven shear stresses remain more than 1 order of magnitude smaller than the primary droplet scale Laplace pressure and the static pressure forces. The measured velocities and inferred flow rates both confirm that the extending oil finger significantly plugs the exit channel [4]. This plugging, in turn, restricts the flows into the exit channel, leading to the buildup of a pressure difference that is released when the droplet is formed through a neck rupturing process that involves a capillary instability. Thus, the first step of forma-

tion of a droplet cannot be explained by a competing mechanism between the shear stress and interfacial tension forces [3–5,9]. It is also not explained by Rayleigh-Plateau capillary instabilities. When the neck begins to form, the finger is shorter than the unstable wavelengths ($\lambda > \pi l$ [16,17]) and the wavelength of the most unstable mode ($\lambda > 5.53l$ [18]). The hydrostatic pressure builds up in the continuous phase inlet channels and squeezes the finger. As the finger is squeezed, it is also slowly stretched, forming a neck significantly smaller than the channel width that shrinks until it rapidly ruptures via a capillary instability. This pinch-off begins when the length of the neck crosses the critical length of the Rayleigh-Plateau instability [17], yielding a primary droplet and a smaller satellite droplet. For example, the cylindrical bridge in Fig. 1(c) has dimensions that will lead to a capillary instability (i.e., the length and radius are 80 and 7.5 μm, respectively). Obviously, micro-PIV provides velocities averaged over a region; in the immediate vicinity of the pinch-off, local instantaneous shear stresses near the moving interfaces can be larger than the spatial average.

This work shows that μPIV and fast imaging of a periodic rupturing phenomenon can be used to obtain detailed information about the flow fields near moving liquid interfaces in microfluidic geometries. Because the boundary conditions of the flow are not always known around these interfaces, a direct μPIV measurement is a convenient way to determine the liquid flows near the interfaces that would not be obvious from simple optical microscopy measurements. These μPIV measurements have focused on looking at the detachment of the primary droplet from the finger; future studies at higher spatial resolution using smaller probe particles are needed to examine the flow fields around the satellite droplet as the neck ruptures. Including tracer particles in the oil phase would also simultaneously reveal flow fields in the dispersed phase. By focusing on slow dripping, this study provides a starting point for extending μPIV measurements in microfluidic devices to the much higher flow rates and capillary numbers that are currently being used in high-throughput droplet production applications. These studies reveal a need for full predictions of the three-dimensional velocity fields and interfacial boundaries of droplets formed by dripping in microfluidic cross channels that have square cross sections.

[1] T. G. Mason and J. Bibette, Langmuir **13**, 4600 (1997); Phys. Rev. Lett. **77**, 3481 (1996).
[2] A. M. Ganan-Calvo, Phys. Rev. Lett. **80**, 285 (1998).
[3] P. Guillot and A. Colin, Phys. Rev. E **72**, 066301 (2005).
[4] P. Garstecki, H. A. Stone, and G. M. Whitesides, Phys. Rev. Lett. **94**, 164501 (2005).
[5] P. Garstecki, I. Gitlin, W. DiLuzio, and G. M. Whitesides, Appl. Phys. Lett. **85**, 2649 (2004).
[6] T. Cubaud and T. G. Mason, Phys. Fluids **20**, 053302 (2008); Phys. Rev. Lett. **96**, 114501 (2006).
[7] S. H. Anna, N. Bontoux, and H. A. Stone, Appl. Phys. Lett. **82**, 364 (2003).
[8] A. M. Ganan-Calvo and J. M. Gordillo, Phys. Rev. Lett. **87**, 274501 (2001).
[9] T. Ward, M. Faivre, M. Abkarian, and H. A. Stone, Electrophoresis **26**, 3716 (2005).
[10] I. Kobayashi, S. Mukataka and M. Nakajima, Langmuir **21**, 7629 (2005).
[11] J. G. Santiago, S. T. Wereley, C. D. Meinhart, D. J. Beebe, and R. J. Adrian, Exp. Fluids **25**, 316 (1998).
[12] H.-C. Chang, Y.-Y. Lin, C.-S. Chern, and S.-Y. Lin, Langmuir **14**, 6632 (1998).
[13] A. S. Utada, A. Fernandez-Nieves, H. A. Stone, and D. A. Weitz, Phys. Rev. Lett. **99**, 094502 (2007).
[14] J. D. Tice, A. D. Lyon and R. F. Ismagilov, Anal. Chim. Acta **507**, 73 (2004).
[15] M. W. Weber and R. Shandas, Microfluid. Nanofluid. **3**, 195 (2007).
[16] L. Rayleigh, Proc. R. Soc. London, Ser. A **10**, 4 (1879).
[17] J. Eggers, Rev. Mod. Phys. **69**, 865 (1997).
[18] S. Tomotika, Proc. R. Soc. London, Ser. A **150**, 322 (1935).